2-Substituted 3-methylnaphtho[1,2-b]furan-4,5-diones as novel L-shaped ortho-quinone substrates for NAD(P)H:quinone oxidoreductase (NQO1)

ARTICLE *in* EUROPEAN JOURNAL OF MEDICINAL CHEMISTRY · MAY 2014

Impact Factor: 3.45 · DOI: 10.1016/j.ejmech.2014.05.041 · Source: PubMed

European Journal of Medicinal Chemistry 82 (2014) 56–67

Contents lists available at ScienceDirect

European Journal of Medicinal Chemistry

journal homepage: http://www.elsevier.com/locate/ejmech

Original article

2-Substituted 3-methylnaphtho[1,2-*b*]furan-4,5-diones as novel L-shaped *ortho*-quinone substrates for NAD(P)H:quinone oxidoreductase (NQO1)

Jinlei Bian [a,c,1], Bang Deng [a,c,1], Lili Xu [a,c], Xiaoli Xu [a,c], Nan Wang [a,c], Tianhan Hu [c], Zeyu Yao [c], Jianyao Du [c], Li Yang [a,c], Yonghua Lei [a,c], Xiang Li [a], Haopeng Sun [a,c], Xiaojin Zhang [a,d,*], Qidong You [a,b,c,**]

[a] Jiangsu Key Laboratory of Drug Design and Optimization, China Pharmaceutical University, Nanjing 210009, China
[b] State Key Laboratory of Natural Medicines, China Pharmaceutical University, Nanjing 210009, China
[c] Department of Medicinal Chemistry, School of Pharmacy, China Pharmaceutical University, Nanjing 210009, China
[d] Department of Organic Chemistry, School of Science, China Pharmaceutical University, Nanjing 210009, China

ARTICLE INFO

Article history:
Received 17 March 2014
Received in revised form
12 May 2014
Accepted 13 May 2014
Available online 14 May 2014

Keywords:
NQO1 substrates
Ortho-quinones
Antitumor
β-Lapachone
Tanshione IIA

ABSTRACT

A series of L-shaped *ortho*-quinone analogs were designed by analyzing the binding mode with NQO1. Metabolic studies demonstrated that compounds **2m**, **2n** and **2q** exhibited higher metabolic rates than β-lapachone. The docking studies, which supported the rationalization of the metabolic studies, constituted a prospective rational basis for the development of optimized *ortho*-quinone analogs. Besides, good substrates (**2m**, **2n** and **2r**) for NQO1 showed higher selective toxicity than β-lapachone toward A549 (NQO1-rich) cancer cells versus H596 (NQO1-deficient) cells. Determination of superoxide ($O_2^{\bullet-}$) production and *in vitro* cytotoxicity evaluation in the presence of the NQO1 inhibitor dicoumarol confirmed that the *ortho*-quinones exerted their antitumor activity through NQO1-mediated ROS production by redox cycling. It was suggested that the L-shaped quinone substrates for NQO1 possessed better specificity and safety than β-lapachone.

1. Introduction

NAD(P)H:quinone oxidoreductase-1 (NQO1) is a dimeric flavoprotein that contains a non-covalently bound molecule of flavin adenine dinucleotide (FAD), and uses the reduced pyridine nucleotide NADH or NADPH as cofactor to catalyze the direct two-electron reduction of a wide variety of quinones [1,2]. Structural biology studies have revealed that NQO1 catalytically cycles using a ping-pong mechanism. In this mechanism, NAD(P)H binds to NQO1, reduces the FAD cofactor to $FADH_2$, and is then released in its oxidized form $NAD(P)^+$, allowing the quinone substrate to bind to the enzyme and to be reduced by $FADH_2$. NQO1-directed bioreduction can turn certain quinone substrates into potent cytotoxic compounds through the formation of unstable hydroquinones that are capable of either alkylating DNA or rapidly generating reactive oxygen species (ROS) through redox cycling [3]. Due to the dramatic elevation of NQO1 in many solid tumors and the little to no expression in normal tissues [4–7], quinone substrates bioreduced by NQO1 to unstable hydroquinones could be potent and selective antitumor agents, which identifies NQO1 as a promising therapeutic target for cancer therapy [8]. Several examples of NQO1 substrates with potent antitumor activity have already been reported in the literature, including the alkylators mitomycin C (MMC), EO9, RH1 and AZQ [9–12] and the redox cycling compounds streptonigrin (STN) [13,14], lavendamycin [15], deoxynyboquinone (DNQ) [12], β-lapachone (β-lap) [16] and tanshinone IIA (TSA) [17] (Fig. 1). Structurally, these substrates fall into two

Abbreviations: NQO1, NAD(P)H:quinone oxidoreductase-1; FAD, flavin adenine dinucleotide; ROS, reactive oxygen species; β-lap, β-lapachone; TSA, tanshinone IIA; MMC, mitomycin C; STN, streptonigrin; DNQ, deoxynyboquinone; PDB, protein data bank; equiv, equivalent; DMSO, dimethyl sulfoxide; MTT, 3-(4,5-dimethylthiazol-2-yl)-2,5-diphe nyltetrazolium bromide; NSCLC, non-small cell lung cancer; DIC, dicoumarol; cyt *c*, cytochrome *c*; MOE, molecular operating environment; SAR, structure–activity relationship; RMSD, root mean square deviation.

* Corresponding author. Jiangsu Key Laboratory of Drug Design and Optimization, China Pharmaceutical University, Nanjing 210009, China.
** Corresponding author. State Key Laboratory of Natural Medicines, China Pharmaceutical University, Nanjing 210009, China.
E-mail addresses: zhangxiaojin@outlook.com (X. Zhang), youqidong@gmail.com (Q. You).
[1] These two authors contributed equally to this work.

http://dx.doi.org/10.1016/j.ejmech.2014.05.041
0223-5234/

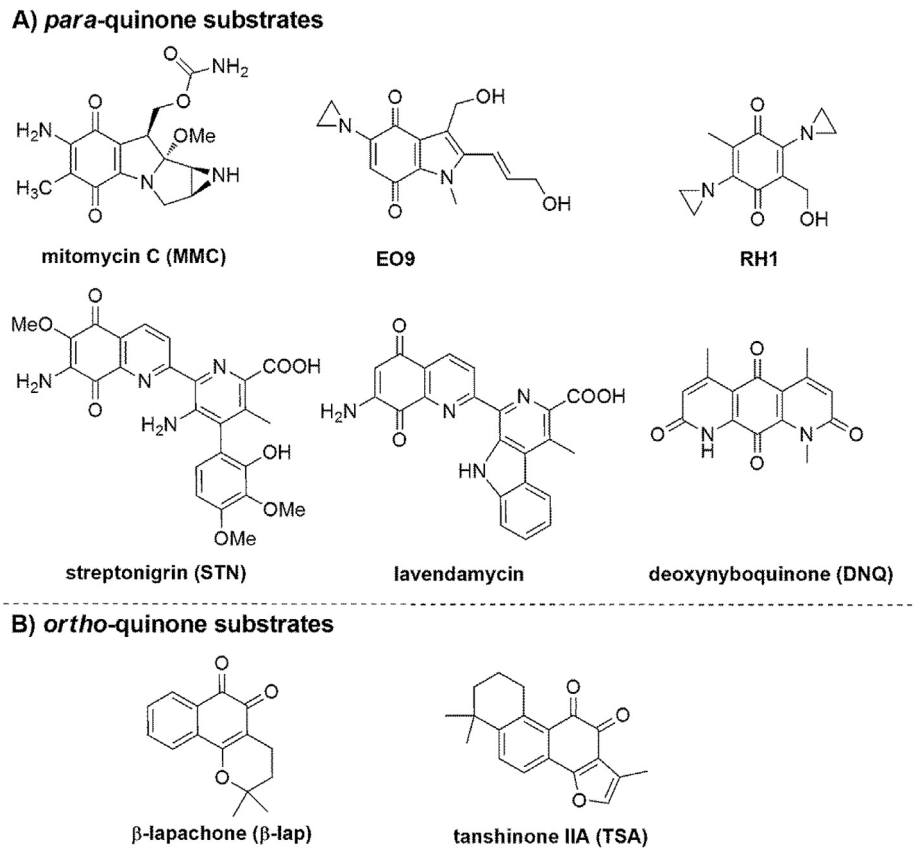

Fig. 1. Several examples of antitumor quinone substrates for NQO1.

main types: *para*-quinones (Fig. 1A) and *ortho*-quinones (Fig. 1B). Compared to the structurally diverse *para*-quinone substrates [9–15], the reported *ortho*-quinone substrates for NQO1 are limited to two natural products, β-lap and TSA. Thus, it is urgent to develop novel and efficient *ortho*-quinone substrates for NQO1 as potent NQO1-directed antitumor agents.

β-Lap (Fig. 1B) is a natural tetrahydropyran-fused *ortho*-naphanoquinone isolated from the *Bignoniaceae* family and is currently in multiple phase II clinical trials for the treatment of pancreatic adenocarcinoma [18]. Unlike conventional chemotherapeutic agents, β-lap has been reported to kill many human cancer cells selectively through rapid ROS generation mediated by NQO1 bioreduction [19]. However, the pyran ring in β-lap is not considered stable as it tends to be hydrolyzed to form ring-opening metabolic products [20], which could result in toxicity to normal tissues and cause side effects. Recently, TSA (Fig. 1B), another natural *ortho*-quinone isolated from *Salvia miltiorrhiza* (Danshen, in Chinese), has also been reported as the substrate for NQO1 [20]. Its structure features a relatively more stable aromatic furan ring fused to the *ortho*-naphanoquinone scaffold as compared to β-lap. In view of this, we initially merged the two natural NQO1 substrates into a new structure of 3-methylnaphtho[1,2-*b*]furan-4,5-dione (**1**) that retained the quinone pharmacophore for NQO1 metabolism (Fig. 2A). This planar structure **1** was then used as a starting point in the design of *ortho*-quinone analogs of β-lap as novel NQO1 substrates. Subsequently, by analyzing the X-ray crystal structure of human NQO1 in complex with its potent competitive inhibitor dicoumarol that obtained from the Protein Data Bank (PDB ID code: 2F1O) [21], we found that the binding site for NQO1 substrates is an L-shaped pocket. Notably, the bound ligand dicoumarol also has an L-type molecular shape that fits well with the L-shaped binding pocket of NQO1 (Fig. 2B). However, the reported *ortho*-quinone substrates and the merged compound **1** are all planar molecules. When docking compound **1** into the binding site of NQO1 using GOLD 5.1 software [22], it has been shown that this planar scaffold only occupied the bottom of the pocket parallel to FAD, but missed the side binding pocket that formed by Tyr128, Phe232, Phe236 and His194 residues (Fig. 2C). In view of this, based on the structural analysis of binding poses of **1** and dicoumarol, we are promoted to introduce nitrogen-containing side chains at the C2 position of **1** using methylene as a linker and to develop L-shaped *ortho*-quinone analogs **2a**–**2s** of β-lap as novel NQO1 substrates (Fig. 2A). The designed L-shaped substrates are expected to have higher specificity for NQO1 and better drug-like properties than the planar compound **1** and β-lap. Herein, we now report the details of a study to identify these L-shaped *ortho*-quinones **2a**–**2s** as efficient NQO1 substrates and examine the effects of the introduced side chains on the metabolism by NQO1 (Fig. 2A). Molecular docking has been applied to analysis the binding modes between the *ortho*-quinone substrates and NQO1, and thus to correlate their metabolic rates with predictions of the key interactions in the catalytic pocket of NQO1. These *ortho*-quinone analogs of β-lap have been tested *in vitro* for their antitumor activity against a pair of NQO1-rich and NQO1-deficient cancer cell lines. In addition, we attempted to confirm whether the *ortho*-quinone analogs exerted their antitumor activity through NQO1-dependent and ROS-mediated pathways.

2. Result and discussion

2.1. Chemistry

The designed 19 *ortho*-quinone target compounds **2a**–**2s** were synthesized in 4–5 steps from commercially available, inexpensive

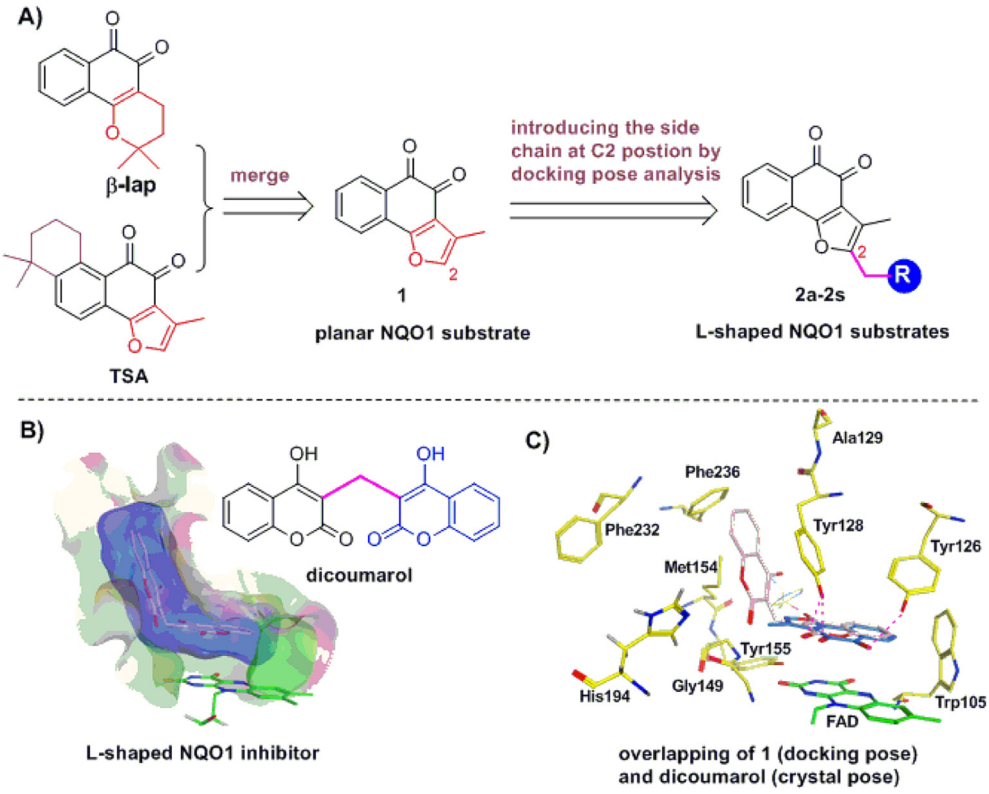

Fig. 2. (A). Designing of novel L-shaped *ortho*-quinone substrates (**2a**–**2s**) for NQO1 by merging the two planar substrates β-lap and TSA and introducing the C2 substituted side chains based on binding pose analysis. (B). Dicoumarol (pink) in the crystal structure (2F1O). The surfaces of protein and ligand were added, respectively. (C) Overlapping of the docking pose of compound **1** (blue) and the crystal pose of dicoumarol (pink) (2F1O). The key residues around the ligands were shown. Hydrogen bonds were shown as dashed lines; the key residues and FAD cofactor were colored in yellow and green, respectively. (For interpretation of the references to colour in this figure legend, the reader is referred to the web version of this article.)

starting materials (Scheme 1). Treatment of 1,4-naphthoquinone with enamine **5**, which prepared from propionaldehyde **3** and morpholine, provided the adduct product **6** in 30% yield. Compound **7** was obtained by heating intermediate **6** in the presence of diluted hydrochloric acid in 78% yield. Oxidation of **7** using the regent Fremy's salt provided the key *ortho*-quinone intermediate **1** in 80% yield. The target compounds **2a**–**2i** that substituted with aliphatic amines were obtained directly through Mannich reaction by the treatment of intermediate **1** with paraformaldehyde and the corresponding aliphatic amines in the acetic acid. The target compounds **2j**–**2s** that substituted with aromatic amine side chains were synthesized by stepwise that involved a chloromethylation of intermediate **1** to form compound **8** and followed by a nucleophilic substitution with corresponding aromatic amines. All of the compounds were confirmed by ^{1}H NMR, IR and HRMS (ESI) spectra, and some representative structures were also confirmed by ^{13}C NMR spectrum.

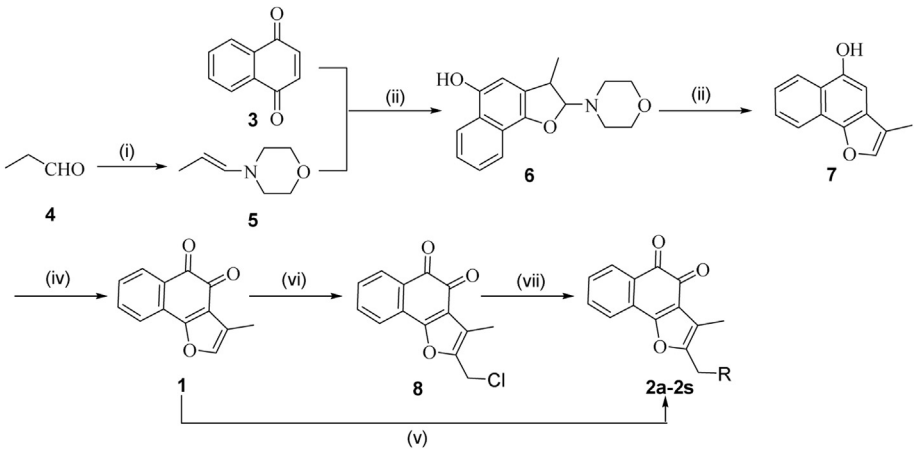

Scheme 1. Reagents and conditions: (i) morpholine, K_2CO_3, 0 °C to rt, 3 h; (ii) CH_2Cl_2, 0 °C to rt, 12 h; (iii) dil. HCl, 75 °C, 3 h; (iv) Fremy's salt, 0 °C, 8 h; (v) $(HCHO)_n$, HOAc, aliphatic amines, 120 °C, 12 h; (vi) $(HCHO)_n$, gaseous HCl, ethyl acetate, 40 °C, 6 h; (vii) aromatic amines, K_2CO_3, KI, acetone, 30 °C, 1 h. For the detailed *R* groups of compounds **2a**–**2s**, see Table 1.

2.2. Measurement of metabolic rates of the ortho-quinone analogs by NQO1

All the *ortho*-quinone analogs of β-lap were evaluated for their ability to act as substrates for NQO1. Although metabolic studies of various *para*-quinones by NQO1 have been reported, there is little of systematic investigation on that of *ortho*-quinone derivatives. To the best of our knowledge, the current work represents the first detailed study of the metabolism of L-shaped *ortho*-quinones by NQO1. The ability of NQO1 to process the *ortho*-quinone analogs of β-lap *in vitro* at the concentration of 10 μmol L^{-1} was assessed. In this assay, the quinone substrate was coincubated with both human NQO1 as well as NADPH. It was capable of quantifying NADPH oxidation to $NADP^+$ by monitoring the absorbance (A_{340} nm) on an enzyme labeling instrument [12]. This method gave initial rates of reduction that could judge directly whether the compounds were good substrates for NQO1 (Fig. 3). Quinone reduction was reversible with the decrease of NADPH, so the results (Table 1) were reported as μmol L^{-1} NADPH oxidized min^{-1} $μmol^{-1}$ NQO1.

As shown in Table 1, generally, most of the L-shaped quinones (**2a**–**2s**) possessed moderate to good metabolic rates by NQO1, indicating that these compounds were good substrates for NQO1. The planar core scaffold (**1**) showed reduced metabolic rate (765 ± 22 μmol NADPH/min/μmol NQO1) as compared to β-lap (1146 ± 22 μmol NADPH/min/μmol NQO1). It was suggested that the replacement of pyran ring with more stable furan ring was disadvantage of elevating the metabolic rate by NQO1. However, most of the C2 substituted L-shaped compounds, such as compounds **2c**, **2d**, **2e**, **2g** and **2k**–**2s**, showed substantially increased metabolic rates by NQO1 relative to the merged planar compound **1**. Among them, compounds **2l**, **2m**, **2n** and **2q** showed even more rapid metabolic rates than β-lap. It suggested that the L-shaped quinones could have higher specificity for NQO1. These results validated our structure-based design ideas in one aspect. Besides, when compared to the aliphatic amine series (**2a**–**2i**) (438–988 μmol NADPH/min/μmol NQO1), the aromatic amine series (**2j**–**2s**) (697–1302 μmol NADPH/min/μmol NQO1) showed much higher metabolic rates in general. This phenomenon was possibly due to the fact that the aromatic group served as a more appropriate moiety to stabilize π-stacking interactions with the key amino acid residues such as Tyr128 and Phe232 in the catalytic site of NQO1 [23]. Among these aromatic amine series, interestingly, all of the compounds **2k**–**2s** with halogen, methyl or methoxy substitution at the benzene moiety exhibited higher metabolic rates (930–1302 μmol NADPH/min/μmol NQO1) than the compound **2j** (697 ± 23 μmol NADPH/min/μmol NQO1) that without any substitution. Furthermore, compounds **2m** and **2q** with chloro substitution at the *para* or *meta* of the aromatic amine moiety, showed higher metabolic rates (1248–1232 μmol NADPH/min/μmol NQO1) than the *ortho*-substituted substrates **2s** (930 ± 95 μmol NADPH/min/μmol NQO1). The fluoro-substituted compound **2n** (1302 ± 180 μmol NADPH/min/μmol NQO1) was slightly better than the corresponding chloro-substituted compound **2m** (1248 ± 57 μmol NADPH/min/μmol NQO1), indicating that fluoro-substitution was a better choice for NQO1 substrates. The compounds **2k**, **2l** and **2r** with a methyl or a methoxy group substituted at the *ortho* or *para* position (1021–1248 μmol NADPH/min/μmol NQO1) showed better metabolic rates than the *meta*-substituted compounds **2o** and **2p** (938–952 μmol NADPH/min/μmol NQO1). This is probably due to the steric interaction effects of the substituents with the residues of the active site. The measurement of metabolic rates of the *ortho*-quinone analogs supported our understanding of the preliminary structure–activity relationships (SAR) of these L-shaped *ortho*-quinone substrates. Overall, compound **2n** with *para*-fluorobenzylamino substitution exhibited the highest metabolic rate (1302 ± 180 μmol NADPH/min/μmol NQO1) by NQO1 and thus it ranked as the best substrate for NQO1. Additionally, over the course of the assay for NQO1 metabolism, it was also observed that each quinone substrate utilized greater than one equiv of NADPH (Table 1), demonstrating the ability of the reduced hydroquinones to be oxidized back to quinones. It suggested that these L-shaped *ortho*-quninoe analogs of β-lap were all good substrates for NQO1 and had antitumor potential by ROS generation via redox cycling (Fig. 3).

Representative compounds **2e**, **2m** and **2n** that showed high metabolic rates at the concentration of 10 μmol L^{-1} were selected to determine their detailed metabolic rates by NQO1 under various

Table 1
Metabolism by NQO1 of *ortho*-quinone analogs and the redox cycles of the process.

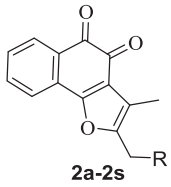

2a-2s

Entry	*R*	Metabolism by NQO1 (μmol NADPH/min/μmol NQO1)	N (cycles)[a]
2a	Me_2N	438 ± 22	7
2b	Et_2N	633 ± 19	10
2c	$(n\text{-}Pr)_2N$	774 ± 65	11
2d	Piperidin-1-yl	988 ± 39	9
2e	Morpholino	950 ± 40	10
2f	Pyrrolidin-1-yl	681 ± 17	11
2g	4-Methylpiperazin-1-yl	790 ± 28	7
2h	4-Acetylpiperzain-1-yl	552 ± 47	9
2i	Cyclohexylamino	678 ± 27	16
2j	PhNH	697 ± 23	15
2k	*p*-MeO-PhNH	1021 ± 94	15
2l	*p*-Me-PhNH	1213 ± 340	15
2m	*p*-Cl-PhNH	1248 ± 57	10
2n	*p*-F-PhNH	1302 ± 180	16
2o	*m*-Me-PhNH	952 ± 44	12
2p	*m*-MeO-PhNH	938 ± 83	11
2q	*m*-Cl-PhNH	1232 ± 225	9
2r	*o*-MeO-PhNH	1083 ± 108	14
2s	*o*-Cl-PhNH	930 ± 95	13
1	–	765 ± 22	10
β-lap	–	1146 ± 23	20

[a] The equiv of NADPH utilized relative to the equiv of substrates over the course of the assay (in 5 min).

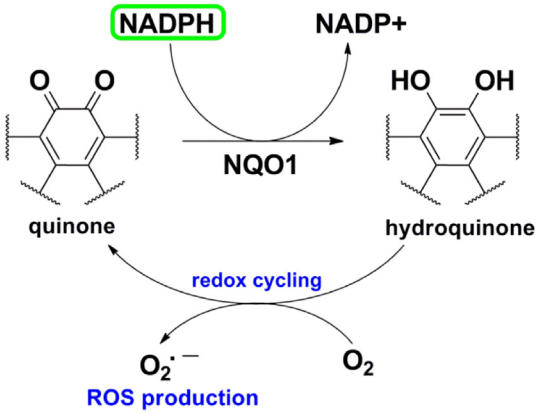

Fig. 3. The principle of the assay for studying quinone metabolism by NQO1.

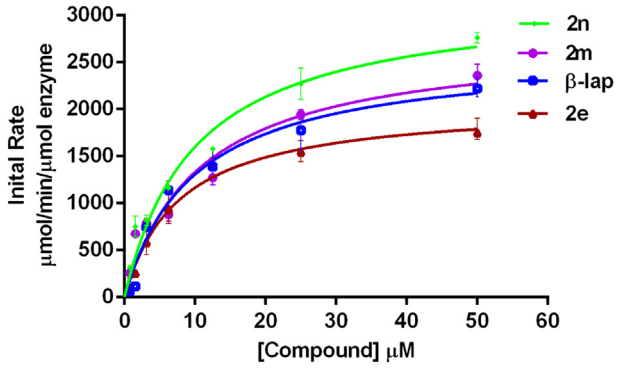

Fig. 4. Michaelis–Menten curves for **2n**, **2m**, **2e** and β-lap with NQO1.

concentrations (0.1–50 μmol L^{-1}). β-Lap was also evaluated as a comparison group. It was shown that the metabolic rates of these quinones by NQO1 increased in a concentration-dependent manner (Fig. 4). According to the data obtained at different concentrations, the corresponding Michaelis–Menten curves for the four substrates were subsequently generated (Fig. 4), and their apparent catalytic efficiencies were calculated. As illustrated in Fig. 4, it was observed that compound **2n** was a highly efficient substrate and redox cycler with a k_{cat}/K_M value of 3.0×10^6 M^{-1} s^{-1}, which was processed much faster than β-lap ($k_{cat}/K_M = 2.6 \times 10^6$ M^{-1} s^{-1}). While compound **2m** ($k_{cat}/K_M = 2.7 \times 10^6$ M^{-1} s^{-1}) showed a slightly higher rate reduced by NQO1 than β-lap. However, for compound **2e** ($k_{cat}/K_M = 2.2 \times 10^6$ M^{-1} s^{-1}) with an aliphatic substitution, exhibited slightly slower metabolic rate than β-lap by NQO1. Obviously, the trends of metabolic rates of the substrates observed in the Michaelis–Menten curves were in accord with that obtained at one concentration of 10 μmol L^{-1}

2.3. Molecular binding pattern study of ortho-quinone substrates with NQO1 by molecular docking

Although several crystal structures of NQO1 in complex with its inhibitors or *para*-quinone substrates were available [23,24], none of crystal structure of NQO1 complex that containing an *ortho*-quinone substrate has ever been reported. Thus, we were prompted to use in silico modeling approach to gain insights into the structural requirements for interactions between the *ortho*-quinone substrates and NQO1. In this work, molecular docking was used to analysis the binding modes of the *ortho*-quinone substrates with NQO1. The *ortho*-quinone compounds were docked into the active site of NQO1 (PDB code 2F1O) using CCDCs software GOLD version 5.1 [25,26]. ChemScore function was explored during the docking experiments. The highest scores represented the best fit for the model.

As shown in Table 2, ChemScore values of the L-shaped compounds were much higher than the planar compounds **1** and β-lap. Among the L-shaped compounds, the aromatic amine series (**2j**–**2s**) showed higher scores than the aliphatic amine series (**2a**–**2i**). The docking scores were well consistent with the metabolism data, suggesting that our model was suitable for the prediction of binding affinities between the *ortho*-quinone substrates and NQO1. All of these *ortho*-quinone compounds could be docked well into the catalytic pocket of NQO1. It indicated that they were all potential substrates for NQO1. The binding modes of these substrates with NQO1 were carefully analyzed and the results for representative compounds (**2a**, **2l**, **2n** and **2p**) were shown in Fig. 5. All of the *ortho*-quinones oriented with the quinone ring above the isoalloxazine ring of the bound cofactor FAD as for hydride transfer by π-stacking interaction, which were similar to the crystal structures of *para*-quinones or inhibitors in complex with NQO1 [23,24]. It was found that the two carbonyl groups in the *ortho*-quinone substrates could bind firmly to the Tyr126 and Tyr128 residues by hydrogen bonding interactions, which was different from the binding mode of *para*-quinone substrates [14]. In addition, there existed an additional pocket formed by Tyr128, Met154, Phe232, Phe236 and His194 for the side chains occupying. As illustrated in Fig. 5, for compounds **2a**, **2l**, **2n** and **2p**, the substituted amine side chains fitted into the additional pocket and the –NH moiety could form another hydrogen bond with S of Met154, providing a rationale for the better activity of the L-shaped compounds compared to the planar structure **1**. Furthermore, analogs with side chains of aromatic amines could fit deep into the pocket and make π-stacking interactions with Tyr128 and Phe232 in the side binding pocket of NQO1. It explained the fact that the aromatic amine analogs exhibited higher metabolic rates by NQO1 than the aliphatic amine analogs. Among the aromatic amine series, all of the compounds **2k**–**2s** with halogen, methyl or methoxy substitution at the benzene moiety provided better scores than the compound **2j** that

Table 2
Computational parameters for selected *ortho*-quinone analogs.

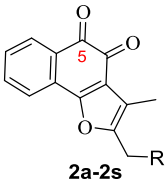

2a-2s

Entry	*R*	ChemScore	C=O5…NH5 (Å)	C=O4…Tyr128OH (Å)	C=O5…Tyr126OH (Å)
2a	Me_2N	79.53	4.00	2.84	2.59
2j	PhNH	89.93	4.07	2.77	2.91
2k	*p*-MeO-PhNH	93.49	4.07	2.92	2.61
2l	*p*-Me-PhNH	91.58	4.10	2.73	2.54
2m	*p*-Cl-PhNH	92.78	4.03	2.89	2.92
2n	*p*-F-PhNH	93.88	3.88	2.89	2.73
2o	*m*-Me-PhNH	91.87	4.03	2.76	2.60
2p	*m*-MeO-PhNH	91.40	4.01	2.91	2.65
1	–	69.68	4.10	2.69	2.89
β-lap	–	67.42	4.04	2.80	2.86

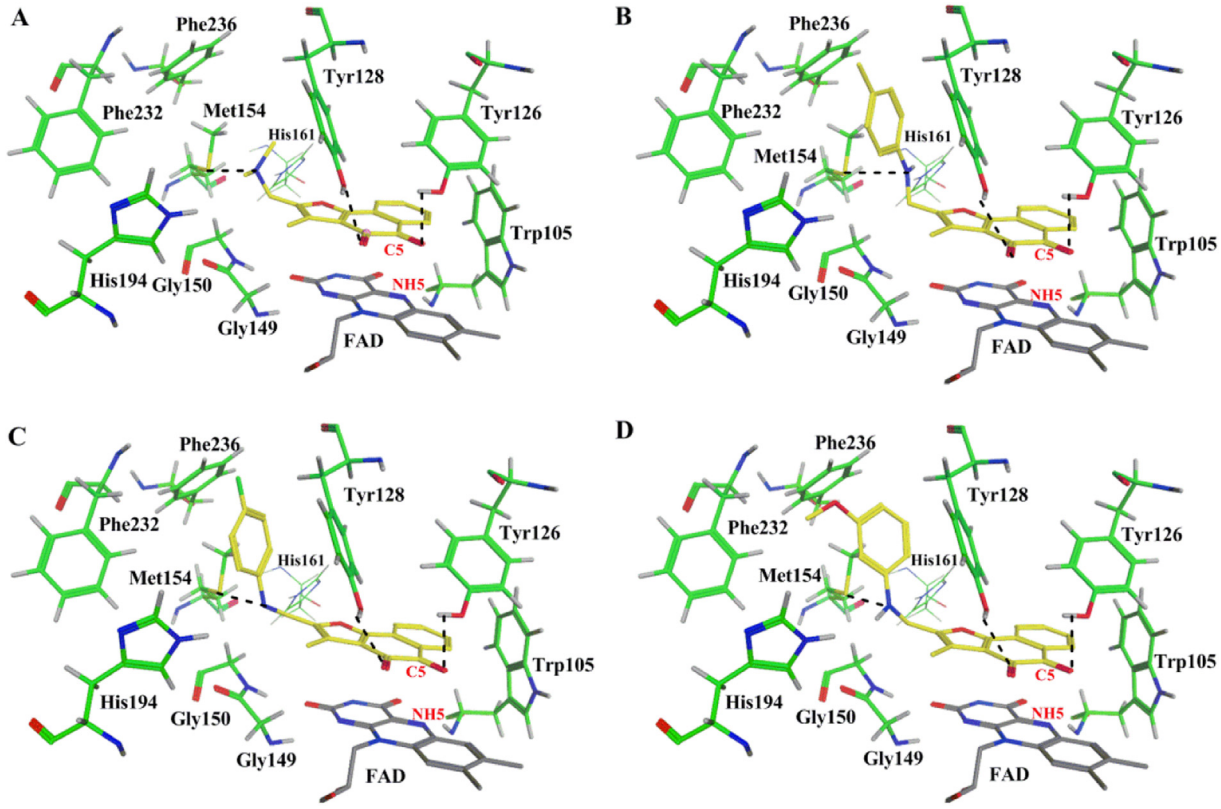

Fig. 5. Docked conformation of compounds **2a** (A), **2l** (B), **2n**(C) and **2p** (D) into active site of NQO1. The interaction mode was obtained through molecular docking (PDB id: 2F1O) and depicted using MOE 2013.08 [29]. The carbon atoms of the compounds and the key residues in the active site of NQO1 were colored in yellow and green, respectively. The H-bonds were shown as black dot lines. (For interpretation of the references to colour in this figure legend, the reader is referred to the web version of this article.)

without any substitution. This could be ascribed to the reduced electron cloud density of the aromatic ring by introduction of halogens, which resulted in enhanced π-stacking interaction with corresponding residues Phe232, Phe236 and Tyr128. As for introducing the methyl group or the methoxy group at the *para* position of the aromatic amine moiety, C–H … π interaction with the adjacent Phe236 residue was observed for enhancing π-stacking interaction with surrounding residues [27]. Moreover, the *meta*-substituted compounds **2o** and **2p** showed slightly worse metabolic rates than the compounds **2k**, **2l**, **2r** and **2s** with substitutions at the *ortho* or *para* position, which was probably due to the steric interaction effects of the substituents with the Met154 residue.

Besides of matching for the catalytic binding site of NQO1, the quinone substrates to be metabolized by NQO1 required an appropriate hydride donor-acceptor distance between the substrate (quinone carbonyl) and the FAD cofactor (atom N5 which transfer the hydride) [28]. In the light of this, the corresponding distances between the *ortho*-quinones and FAD were calculated and analyzed. As shown in Table 2, all were within a reasonable distance (about 4 Å) for hydride transfer from the reduced FAD ($FADH_2$) to quinone substrates. In addition, the hydrogen bonding interactions of C═O4 … Tyr128OH and C═O5 … Tyr126OH were suggested to reduce the electron cloud density of the carbonyl groups, thus promoting the hydride transfer from the $FADH_2$ to the *ortho*-quinone.

2.4. In vitro cytotoxicity evaluation

Cytotoxicity studies were performed on all the *ortho*-quinone analogs of β-lap with cell survival being determined by the 3-(4, 5-dimethylthiazol-2-yl)-2,5-diphenyltetrazolium bromide (MTT) colorimetric assay against the human non-small cell lung cancer (NSCLC) cell lines, A549 (NQO1-rich) and H596 (NQO1-deficient) cells. β-Lap was used as positive control. The MTT assay was dependent on the reduction of tetrazolium salt by the mitochondrial dehydrogenase of viable cells to form a blue formazan product dissolved in DMSO and measured at 560 nm. The results of cytotoxic activity *in vitro* were expressed as the IC_{50}, and selectivity ratios were defined as IC_{50} value for the H596 cell line divided by IC_{50} value for the A549 cell line (Table 3).

As shown in Table 3, it was found that all the compounds excepted for **2p** showed moderate to potent cytotoxicity against NQO1-rich A549 cell line with IC_{50} values ranging from 2.2 to 35 μmol L^{-1}. Nearly half of the analogs possessed comparative cytotoxicity to the positive control β-lap with IC_{50} values less than 10 μmol L^{-1} against A549 cell line. On the contrary, generally, the compounds showed relative poor cytotoxicity against NQO1-deficient H596 cell line. It suggested that these NQO1 substrates were more sensitive to NQO1-rich cancer cells. Interestingly, compound **1** with slower metabolic rate by NQO1 compared to β-lap also exhibited a poorer selectivity (selectivity ratio = 1.4) than that of β-lap (selectivity ratio = 4.0). Nevertheless, most of the L-shaped compounds showed better toxic selectivity to NQO1-rich A549 cell line compared to the planar compound **1**. Furthermore, it was also observed that the aromatic amine series generally possessed higher selectivity ratios than the aliphatic amine series. Especially, among the aromatic amine series, compounds **2m**, **2n**, **2q** and **2r** even showed better toxic selectivity to NQO1-rich A549 cell line versus NQO1-deficient H596 cell line (selectivity ratio ≥5.3) compared to the control β-lap (selectivity ratio = 4.0). It must be emphasized that these four *ortho*-quinones were all efficient substrates for NQO1 with metabolic rates more than

Table 3
Cytotoxicity of *ortho*-quinone analogs toward A549 (NQO1-rich) and H596 (NQO1-deficient) cell lines.

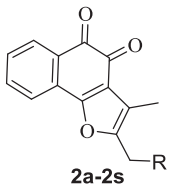

2a-2s

Entry	*R*	Cytotoxicity IC_{50} (μmol L^{-1})		Selectivity ratio IC_{50} (H596)/IC_{50} (A549)
		A549	H596	
2a	Me_2N	2.3 ± 0.1	3.8 ± 0.6	1.7
2b	Et_2N	16 ± 1.2	11 ± 0.2	0.7
2c	$(n\text{-}Pr)_2N$	20 ± 3.4	34 ± 4.0	1.7
2d	Piperidin-1-yl	12 ± 3.7	10 ± 0.5	0.8
2e	Morpholino	10 ± 2.4	30 ± 2.1	3.0
2f	Pyrrolidin-1-yl	4.9 ± 2.0	21 ± 3.6	4.3
2g	4-Methylpiperazin-1-yl	2.2 ± 0.4	4.8 ± 2.2	2.2
2h	4-Acetylpiperzain-1-yl	29 ± 5.5	14 ± 0.8	0.5
2i	Cyclohexylamino	35 ± 6.6	34 ± 5.4	1.0
2j	PhNH	31 ± 2.9	>50	>1.6
2k	*p*-MeO-PhNH	19 ± 3.5	>50	>2.6
2l	*p*-Me-PhNH	11 ± 2.6	13 ± 1.0	1.2
2m	*p*-Cl-PhNH	4.9 ± 0.9	28 ± 1.6	5.7
2n	*p*-F-PhNH	6.0 ± 0.3	>50	>8.3
2o	*m*-Me-PhNH	14 ± 1.5	49 ± 8.1	3.5
2p	*m*-MeO-PhNH	>50	>50	–
2q	*m*-Cl-PhNH	4.7 ± 0.3	25 ± 2.0	5.3
2r	*o*-MeO-PhNH	9.2 ± 1.0	>50	>5.4
2s	*o*-Cl-PhNH	6.4 ± 2.2	25 ± 3.6	3.9
1	–	7.4 ± 1.6	10 ± 3.5	1.35
β-lap	–	5.7 ± 1.1	23 ± 5.1	4.0

1000 μmol NADPH/min/μmol NQO1. Notably, compound **2n** that showed the highest metabolic rate also afforded the greatest selectivity to NQO1-rich A549 cell line (more than 8.3-fold). Compound **2n** was as potent as the positive control β-lap against A549 cell line with an IC_{50} value of 6.0 ± 0.3 μmol L^{-1}. Meanwhile, compound **2n** showed much less toxic against H596 cell line even at a high concentration of 50 μmol L^{-1}. These results revealed that good substrates for NQO1 were selectivity toxic towards cell line with high NQO1 activity, which was consistent with that reported previously in the literature [13]. In addition, it is worth noting that the L-shaped *ortho*-quinones including **2n**, **2m**, **2q** and **2r**, which showed better selectivity than β-lap against NQO1-rich cancer cells, were supposed to have a superior safety profile since there was little or no NQO1 expressed in normal tissues. These novel L-shaped *ortho*-quinones could be promising NQO1-directed antitumor agents for further preclinical studies.

2.5. Determination of ROS production

NQO1 substrates have been suggested to arise their antitumor activity through rapid ROS generation [20]. We have found that each *ortho*-quinone substrate utilized greater than one equiv NADPH (Table 1), demonstrating their ability of the redox cycling. Considering that the redox cycling could led to ROS generation (Fig. 3), we thus selected representative compounds (**2m**, **2n** and **2q**) with efficient metabolic rates to further identify their abilities to produce ROS. Menadione, a well-studied *para*-quinone substrate for NQO1 was used as positive control [30]. The production of the superoxide ($O_2^{\cdot-}$), the main constitute of ROS, was measured by a spectrophotometric assay using cytochrome *c* as the terminal electron acceptor [31]. The initial rates (μmol cytochrome *c* reduced/min/mg NQO1) were calculated from the liner portion (0–30 s) of the reduction graphs. The highest value represented it can produce maximum amount of ROS. As shown in Fig. 6, the L-shaped *ortho*-quinones **2m**, **2n** and **2q** showed rapid rates of ROS generation, being much more efficient than β-lap. Compound **2n** with the highest metabolic rate by NQO1 (1302 ± 180 μmol NADPH/min/μmol NQO1) also exhibited the highest rate of ROS production (1198 ± 20 μmol cyt *c*/min/mg NQO1) (Fig. 6). In fact, the rate of ROS production for compound **2n** was comparable to that of the positive control menadione (1315 ± 25 μmol cyt *c*/min/mg NQO1). The results indicated that these *ortho*-quinone substrates could generate a high level of ROS via NQO1-directed redox cycling.

2.6. Antitumor effect of **2n** is NQO1-dependent and ROS-mediated

The best selective compound **2n** was further tested in the presence of the NQO1 inhibitor dicoumarol (DIC, 25 μmol L^{-1}) for its rate of ROS production and toxicity against A549 cell line (Fig. 7). DIC has been widely used in studies of NQO1-mediated cell death, as incubation of cells with the inhibitor was effective in blocking the enzymatic activity of NQO1 [12]. As illustrated in Fig. 7A, coincubation with DIC dramatically reduced the rate of ROS production by **2n**. Fig. 7B showed that coincubation with DIC greatly protected A549 cells from the cell death mediated by **2n**, shifting the IC_{50} > 12-fold. (The fold is the ratio of the IC_{50} of cotreatment with quinone and DIC to the IC_{50} of treatment with only quinone, and a higher ratio indicates greater protection and greater NQO1 specificity). At the concentration of 10 μmol L^{-1}, **2n** killed about half of the cells while scarcely dead cells were observed in the presence of NQO1 inhibitor dicoumarol. The results suggested that the *ortho*-quinone analogs exerted their antitumor activity through NQO1-dependent and ROS-mediated pathways.

3. Conclusion

In summary, a key scaffold of 3-methylnaphtho[1,2-*b*]furan-4,5-diones was merged from two natural *ortho*-quinone products, β-lap and TSA. Based on the scaffold, a series of L-shaped *ortho*-quinone analogs with substituted side chains at the position of C2 were designed by analyzing the binding mode with NQO1. These *ortho*-quinones have been characterized and evaluated as efficient substrates for recombinant human NQO1. The C2-substituted L-shaped compounds showed substantially increased metabolic rates by NQO1 relative to the planner structure **1** (765 ± 22 μmol NADPH/min/μmol NQO1). Compounds **2m**, **2n** and **2q** with halogen

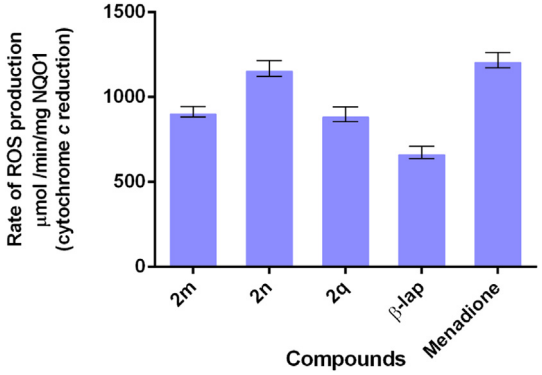

Fig. 6. Rate of ROS production of representative compounds (**2m**, **2n** and **2q**), β-lap and menadione and rates are expressed as mean ± SD, $P < 0.001$ versus control ($n = 3$). (Spectrophotometric assay with cytochrome *c* as terminal electron acceptor (550 nm)).

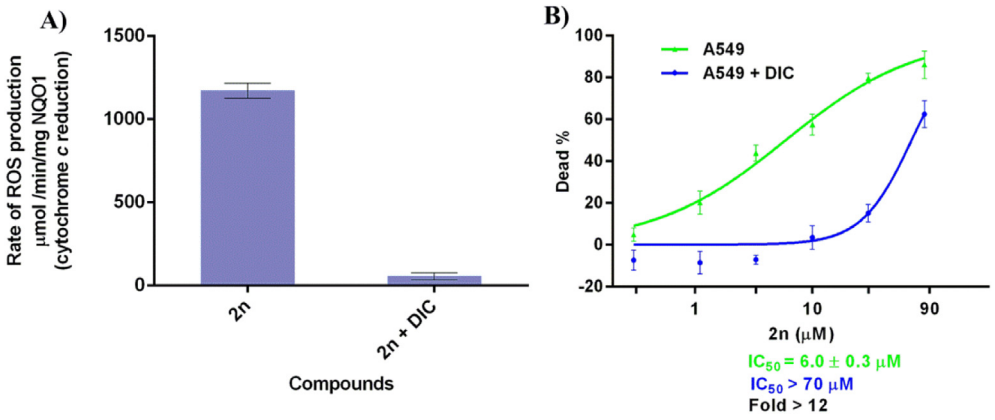

Fig. 7. (A) Rate of ROS production of **2n** in the presence and absence of the NQO1 inhibitor (DIC, 25 µmol L^{-1}) with NQO1 and rates are expressed as mean ± SD, $P < 0.001$ versus control ($n = 3$). (Spectrophotometric assay with cytochrome *c* as terminal electron acceptor (550 nm)). (B) Cell death of A549 cells treated for 2 h with **2n** in the presence and absence of the NQO1 inhibitor (DIC, 25 µmol L^{-1}). IC_{50} values and Fold are listed blew the graphs with standard error ($n \geq 3$). The Fold is (IC_{50} values with DIC/IC_{50} of quinone alone).

substitution at the *meta* or *para* of aromatic amines exhibited higher metabolic rates (1248–1302 µmol NADPH/min/µmol NQO1) than the control β-lap (1146 ± 23 µmol NADPH/min/µmol NQO1). Molecular modeling was used to analyze the interactions between the *ortho*-quinone substrates and NQO1. Our docking studies supported the rationalization of the metabolic study and constituted a prospective rational basis for the development of optimal *ortho*-quinone analogs. Besides, good substrates (**2m**, **2n** and **2r**, metabolism rates > 1000 µmol NADPH/min/µmol NQO1) for NQO1 showed higher selective toxicity than β-lap toward A549 (NQO1-rich) cell line versus H596 (NQO1-deficient) cell line. Determination of superoxide ($O_2^{\cdot-}$) production and *in vitro* cytotoxicity evaluation in the presence of the NQO1 inhibitor dicoumarol confirmed that the *ortho*-quinone analogs of β-lap exerted their antitumor activity through NQO1-mediated ROS production via redox cycling. Compound **2n** (named as **YK-01**), in which an encouraging improvement of better enzyme activity, more selectivity and superior safety profile as compared to β-lap, can be considered as a lead chemotype worth of further investigations toward the design and synthesis of novel NQO1-directed antitumor *ortho*-quinones. These findings encourage further investigations around this interesting antitumor chemotype.

4. Experimental

4.1. Chemistry

All reagents were purchased from commercial sources. Organic solutions were concentrated in a rotary evaporator (BüchiRotavapor) below 55 °C under reduced pressure. Reactions were monitored by thin-layer chromatography (TLC) on 0.25 mm silica gel plates (GF254) and visualized under UV light. Melting points were determined with a Melt-Temp II apparatus. The ^{1}H NMR and ^{13}C NMR spectra were measured on a Bruker AV-300 instrument using deuterated solvents with tetramethylsilane (TMS) as internal standard. IR spectra were recorded on a Nicolet iS10 Avatar FT-IR spectrometer using KBr film. EI-MS was collected on shimadzu GCMS-2010 instruments. ESI-mass and high resolution mass spectra (HRMS) were recorded on a Water Q-Tofmicro mass spectrometer. Analytical results are within 0.40% of the theoretical values.

4.1.1. (*E*)-4-(Prop-1-en-1-yl)morpholine (**5**)

To a stirred mixture of morpholine (26 mL, 0.294 mol) and anhydrous K_2CO_3 (2.0 g, 14.7 mmol) was added dropwise propanal (9 mL, 0.125 mol) at 0 °C. The suspension was stirred at 0 °C for 2 h and then warmed to room temperature in about 1 h. The reaction mixture was filtered and washed with dimethyl ether (2 × 20 mL). The filtration was concentrated to give a dark color liquid, which was purified by vacuum distillation to give the titled compound as a colorless liquid (7.0 g, 45%). b.p. 88–90 °C/25 mm [32]. ^{1}H NMR (300 MHz, DMSO) δ: 5.83 (d, 1H, $J = 15$ Hz), 4.38 (dq, 1H, $J = 12$ Hz, 9 Hz), 3.58–3.50 (m, 4H), 2.85–2.75 (m, 2H), 2.52–2.44 (m, 2H), 1.60–1.53 (m, 3H). *m/z* (EI-MS): 127 $[M]^+$.

4.1.2. 3-Methyl-2-morpholino-5-hydroxy-2,3-dihydronaphtho[1,2-b]furan (**6**)

To a solution of naphthoquinone **3** (7.3 g, 46.25 mmol) in dry dichloromethane (150 mL) was added **5** (5.9 g, 46.25 mmol) at 0 °C. The reaction mixture was then warmed to room temperature and kept for 12 h. The precipitate was filtered, washed with dichloromethane (2 × 10 mL), and dried to give the titled compound as a while solid (4.0 g, 30%). m.p. 141–143 °C. ^{1}H NMR (300 MHz, DMSO) δ: 9.48 (s, 1H), 8.03 (d, 1H, $J = 7.8$ Hz), 7.76 (d, 1H, $J = 7.7$ Hz), 7.44–7.35 (m, 2H), 6.70 (s, 1H), 5.11 (d, 1H, $J = 4.8$ Hz), 3.54 (s, 4H), 3.43–3.40 (m, 1H), 2.82–2.75 (m, 2H), 2.57–2.53 (m, 2H), 1.28 (d, 3H, $J = 6.9$ Hz). *m/z* (EI-MS): 285 $[M]^+$.

4.1.3. 3-Methyl-5-hydroxynaphthol[1,2-b]furan (**7**)

To a solution of **6** (3.5 g, 12.37 mmol) in THF (20 mL) was added diluted hydrochloric acid (5%, 90 mL). The reaction mixture was refluxed for 2 h, and then cooled and extracted by ethyl acetate (3 × 30 mL). The organic layers were combined, dried over anhydrous Na_2SO_4 and concentrated to give a light pink solid, which was further purified by recrystallization from dichloromethane to give the titled compound as a white solid (1.9 g, 78%). m.p. 145–147 °C. ^{1}H NMR (300 MHz, $CDCl_3$) δ: 8.25–8.22 (m, 2H), 7.61 (t, 1H, $J = 8.0$ Hz), 7.53–7.47 (m, 2H), 6.94 (s, 1H), 5.06 (s, 1H), 2.27 (s, 3H). *m/z* (EI-MS): 198 $[M]^+$.

4.1.4. 3-Methylnaphtho[1,2-b]furan-4,5-dione (**1**)

To a solution of **7** (400 mg, 2.03 mmol) in acetone (10 mL) was added a 0.65 M potassium dihydrogenphosphate aqueous solution (100 mL). The reaction mixture was stirred at room temperature for 12 h. After that, the acetone was evaporated under reduced pressure, giving a red precipitate. The precipitate was then collected and purified by recrystallization from ethanol to give the titled compound as a red solid (2.2 g, 80%). m.p. 170–172 °C. ^{1}H NMR (300 MHz, $CDCl_3$) δ: 8.09 (d, 1H, $J = 7.8$ Hz), 7.69–7.62 (m, 2H), 7.47 (t, 1H, $J = 9.0$ Hz), 2.31 (s, 3H). IR (ν, cm^{-1}): 3134, 1672, 1590, 1539,

1020. ESI-HRMS *m/z* $[M+Na]^+$ calculated for $C_{13}H_8O_3Na$: 235.0371, found: 235.0374.

*4.1.5. General procedure for the preparation of compounds **2a–2i***

A mixture of naphthoquinone **1** (130 mg, 0.61 mmol), paraformaldehyde (73 mg, 0.244 mmol) and the corresponding aliphatic amines (1.22 mmol) in acetic acid (10 mL) was stirred at room temperature until the initial reactant **1** disappeared by TLC control. Then, the solvent was vacuum-evaporated and the residue was redissolved in ethyl acetate. The organic layer was washed with saturated $NaHCO_3$ aqueous and brine, dried over anhydrous Na_2SO_4, filtrated and concentrated to afford a crude product, which was purified through column chromatography over silica gel.

*4.1.5.1. 2-((Dimethylamino)methyl)-3-methylnaphtho[1,2-b]furan-4,5-dione (**2a**).* Following the above procedure, treatment of **1** with dimethylamine for 12 h under reflux, gave the crude product, which was purified by column chromatography (eluent: Petroleum ether/EtOAc 10:1) to afford **2a** as an orange solid (51 mg, 31%). m.p. 140–142 °C. ^{1}H NMR (300 MHz, DMSO) δ: 7.89 (d, J = 7.6 Hz, 1H), 7.69 (d, J = 10.2 Hz, 2H), 7.51 (d, J = 7.5 Hz, 1H), 3.48 (s, 2H), 2.18 (s, 9H). ^{13}C NMR (75 MHz, $CDCl_3$) δ: 180.3, 175.1, 159.1, 150.5, 134.7, 129.8, 129.4, 128.3, 128.1, 122.0, 121.1, 118.8, 52.6, 44.6, 8.4. IR (ν, cm^{-1}): 2933, 1667, 1581, 1214, 906. ESI-HRMS *m/z* $[M+H]^+$ calculated for $C_{16}H_{16}NO_3$: 270.1130, found: 270.1132.

*4.1.5.2. 2-((Diethylamino)methyl)-3-methylnaphtho[1,2-b]furan-4,5-dione (**2b**).* Following the above procedure, treatment of **1** with dimethylamine for 12 h under reflux, gave the crude product, which was purified by column chromatography (eluent: Petroleum ether/EtOAc 2:1) to afford **2b** as a red solid (65 mg, 36%). m.p. 149–151 °C. ^{1}H NMR (300 MHz, DMSO) δ: 7.90 (d, J = 7.4 Hz, 1H), 7.72–7.63 (m, 2H), 7.50 (t, J = 7.5 Hz, 1H), 3.66 (s, 2H), 2.52 (dd, J = 6.7, 4.6 Hz, 4H), 2.19 (s, 3H), 1.05–1.00 (m, 6H). ^{13}C NMR (75 MHz, $CDCl_3$) δ: 180.1, 175.1, 159.2, 151.0, 134.8, 129.8, 129.4, 128.3, 128.1, 121.9, 121.0, 118.8, 58.7, 46.4, 11.2, 8.5. IR (ν, cm^{-1}): 2918, 1675, 1581, 1216, 1109. ESI-HRMS *m/z* $[M+H]^+$ calculated for $C_{18}H_{20}NO_3$: 298.1443, found: 298.1439.

*4.1.5.3. 2-((Dipropylamino)methyl)-3-methylnaphtho[1,2-b]furan-4,5-dione (**2c**).* Following the above procedure, treatment of **1** with dipropylamine for 6 h under reflux, gave the crude product, which was purified by column chromatography (eluent: Petroleum ether/EtOAc 4:1) to afford **2c** as a red solid (54 mg, 27%). m.p. 153–155 °C. ^{1}H NMR (300 MHz, $CDCl_3$) δ: 8.07 (d, J = 7.7 Hz, 1H), 7.71–7.61 (m, 2H), 7.44 (t, J = 7.5 Hz, 1H), 3.68 (s, 2H), 2.49–2.44 (m, 4H), 2.29 (s, 3H), 1.55 (dq, J = 14.7, 7.4 Hz, 4H), 0.93 (t, J = 7.3 Hz, 6H). ^{13}C NMR (75 MHz, $CDCl_3$) δ: 180.4, 175.1, 159.1, 149.9, 134.8, 129.8, 129.3, 128.3, 128.1, 121.7, 121.2, 119.3, 55.3, 47.1, 19.5, 11.3, 8.5. IR (ν, cm^{-1}): 3414, 2959, 1673, 1554, 1216, 1081, 905. ESI-HRMS *m/z* $[M+H]^+$ calculated for $C_{20}H_{24}NO_3$: 326.1756, found: 326.1752.

*4.1.5.4. 2-(Piperidin-1-ylmethyl)-3-methylnaphtho[1,2-b]furan-4,5-dione (**2d**).* Following the above procedure, treatment of **1** with piperidine for 12 h under reflux, gave the crude product, which was purified by column chromatography (eluent: Petroleum ether/EtOAc 10:1) to afford **2d** as a red solid (38 mg, 20%). m.p. 154–157 °C. ^{1}H NMR (300 MHz, $CDCl_3$) δ: 8.06 (d, J = 7.7 Hz, 1H), 7.76 (d, J = 7.7 Hz, 1H), 7.63 (t, J = 7.6 Hz, 1H), 7.44 (t, J = 7.6 Hz, 1H), 3.71 (s, 2H), 2.64 (s, 4H), 2.30 (s, 3H), 1.85 (s, 6H). ^{13}C NMR (75 MHz, $CDCl_3$) δ: 180.4, 175.1, 159.0, 150.4, 134.7, 129.8, 129.3, 128.3, 128.2, 122.0, 121.2, 118.9, 53.7, 52.4, 25.3, 23.5, 8.6. IR (ν, cm^{-1}): 2935, 1669, 1650, 1216, 907. ESI-HRMS *m/z* $[M+H]^+$ calculated for $C_{19}H_{20}NO_3$: 310.1443, found: 310.1449.

*4.1.5.5. 2-(Morpholinomethyl)-3-methylnaphtho[1,2-b]furan-4,5-dione (**2e**).* Following the above procedure, treatment of **1** with morpholine for 12 h under reflux, gave the crude product, which was purified by column chromatography (eluent: Petroleum ether/EtOAc 4:1) to afford **2e** as a red solid (57 mg, 30%). m.p. 170–171 °C. ^{1}H NMR (300 MHz, $CDCl_3$) δ: 8.05 (d, J = 7.5 Hz, 1H), 7.73 (d, J = 7.2 Hz, 1H), 7.62 (t, J = 4.8 Hz, 1H), 7.45 (t, J = 7.2 Hz, 1H), 3.73 (s, 4H), 3.58 (s, 2H), 2.54 (s, 4H), 2.28 (s, 3H). ^{13}C NMR (75 MHz, $CDCl_3$) δ: 180.2, 174.9, 159.0, 149.6, 134.8, 129.8, 129.4, 128.2, 128.0, 121.9, 121.1, 119.2, 66.3, 52.7, 52.0, 8.5. IR (ν, cm^{-1}): 3432, 2857, 1668, 1578, 1111, 908. ESI-HRMS *m/z* $[M+Na]^+$ calculated for $C_{18}H_{17}NO_4Na$: 334.1055, found: 334.1057.

*4.1.5.6. 2-(Pyrrolidin-1-ylmethyl)-3-methylnaphtho[1,2-b]furan-4,5-dione (**2f**).* Following the above procedure, treatment of **1** with tetrahydropyrrole for 12 h under reflux, gave the crude product, which was purified by column chromatography (eluent: Petroleum ether/EtOAc 4:1) to afford **2f** as a dark red solid (36 mg, 20%). m.p. 150–151 °C. ^{1}H NMR (300 MHz, $CDCl_3$) δ 8.06 (d, J = 7.7 Hz, 1H), 7.76 (d, J = 7.7 Hz, 1H), 7.63 (t, J = 7.6 Hz, 1H), 7.44 (t, J = 7.6 Hz, 1H), 3.71 (s, 2H), 2.64 (s, 4H), 2.30 (s, 3H), 1.85 (s, 4H). ^{13}C NMR (75 MHz, $CDCl_3$) δ: 180.2, 175.1, 159.2, 148.4, 134.8, 129.8, 129.5, 128.3, 128.0, 122.0, 121.1, 118.8, 53.3, 48.4, 23.0, 8.5. IR (ν, cm^{-1}): 3221, 2757, 1678, 1578, 1032, 900. ESI-HRMS *m/z* $[M+H]^+$ calculated for $C_{18}H_{18}NO_3$: 296.1287, found: 296.1292.

*4.1.5.7. 2-((4-Methylpiperazin-1-yl)methyl)-3-methylnaphtho[1,2-b]furan-4,5-dione (**2g**).* Following the above procedure, treatment of **1** with *N*-methylpiperazine for 12 h under reflux, gave the crude product, which was purified by column chromatography (eluent: Petroleum ether/EtOAc 4:1) to afford **2g** as a red solid (30 mg, 15%). m.p. 160–162 °C. ^{1}H NMR (300 MHz, $CDCl_3$) δ: 8.06 (d, J = 8.9 Hz, 1H), 7.74 (d, J = 7.0 Hz, 1H), 7.63 (t, J = 7.6 Hz, 1H), 7.44 (t, J = 7.6 Hz, 1H), 3.62 (s, 2H), 2.52–2.39 (m, 4H), 2.32–2.29 (m, 7H), 2.10 (s, 3H). ^{13}C NMR (75 MHz, $CDCl_3$) δ: 180.2, 174.9, 159.0, 150.0, 134.7, 129.8, 129.4, 128.2, 128.0, 121.9, 121.1, 119.1, 54.3, 52.1, 51.6, 45.3, 8.5. IR (ν, cm^{-1}): 3423, 2795, 1667, 1577, 1292, 1216, 907, 786. ESI-HRMS *m/z* $[M+H]^+$ calculated for $C_{19}H_{21}N_2O_3$: 325.1547, found: 325.1553.

*4.1.5.8. 2-((4-Acetylpiperazin-1-yl)methyl)-3-methylnaphtho[1,2-b]furan-4,5-dione (**2h**).* Following the above procedure, treatment of **1** with *N*-acetylpiperazine for 12 h under reflux, gave the crude product, which was purified by column chromatography (eluent: Petroleum ether/EtOAc 4:1) to afford **2h** as a red solid (54 mg, 25%). m.p. 168–170 °C. ^{1}H NMR (300 MHz, $CDCl_3$) δ: 8.07 (d, J = 8.9 Hz, 1H), 7.74 (d, J = 6.6 Hz, 1H), 7.63 (t, J = 7.6 Hz, 1H), 7.46 (t, J = 6.6 Hz, 1H), 3.72–3.67 (m, 2H), 3.62 (s, 2H), 3.51 (d, J = 4.5 Hz, 2H), 2.54 (t, J = 9.2 Hz, 4H), 2.28 (s, 3H), 2.10 (s, 3H). ^{13}C NMR (75 MHz, $CDCl_3$) δ: 180.2, 174.9, 168.1, 159.0, 149.9, 134.7, 129.8, 129.4, 128.2, 128.0, 121.9, 121.1, 119.1, 52.1, 51.6, 49.1, 20.8, 8.5. IR (ν, cm^{-1}): 3323, 2935, 1700, 1569, 1216, 979. ESI-HRMS *m/z* $[M+H]^+$ calculated for $C_{20}H_{21}N_2O_4$: 353.1501, found: 353.1503.

*4.1.5.9. 2-((Cyclohexylamino)methyl)-3-methylnaphtho[1,2-b]furan-4,5-dione (**2i**).* Following the above procedure, treatment of **1** with cyclohexylamine for 12 h under reflux, gave the crude product, which was purified by column chromatography (eluent: Petroleum ether/EtOAc 4:1) to afford **2i** as a dark red solid (55 mg, 28%). m.p. 163–165 °C. ^{1}H NMR (300 MHz, $CDCl_3$) δ: 8.06 (d, J = 7.2 Hz, 1H), 7.74 (d, J = 6.6 Hz, 1H), 7.63 (t, J = 7.6 Hz, 1H), 7.46 (t, J = 6.6 Hz, 1H), 3.87 (s, 2H), 2.50–2.49 (m, 1H), 2.28 (s, 3H), 1.96–1.94 (m, 2H), 1.75–1.67 (m, 4H), 1.26–1.13 (m, 4H). ^{13}C NMR (75 MHz, $CDCl_3$) δ: 180.4, 175.1, 159.0, 150.4, 134.7, 129.8, 129.3, 128.3, 128.2, 122.0, 121.2, 118.9, 57.3, 43.5, 34.7, 25.9, 25.3, 8.6. IR (ν, cm^{-1}): 3233, 2915,

1650, 1759, 1134, 988. ESI-HRMS *m/z* $[M+H]^+$ calculated for $C_{20}H_{22}NO_3$: 324.1600, found: 324.1601.

*4.1.6. 2-Chloromethyl-3-methylnaphtho[1,2-b]furan-4,5-dione (**8**)*

Gaseous hydrogen chloride was filled into a solution of quinone **1** (100 mg, 0.47 mmol) and paraformaldehyde (138 mg, 4.7 mmol) in ethyl acetate (8 mL). The reaction mixture was stirred at 45–50 °C for 5 h. Then, the solvent was vacuum-evaporated and the residue was redissolved in ethyl acetate. The organic layer was washed with brine, dried Na_2SO_4, filtered and evaporated till dryness, affording a crude product, which was purified through column chromatography over silica gel to give 98 mg of the red product. Yield 80%, m.p. 158–159 °C. ^{1}H NMR (300 MHz, $CDCl_3$) δ: 8.10 (d, J = 7.7 Hz, 1H), 7.77 (d, J = 7.3 Hz, 1H), 7.68 (t, J = 7.5 Hz, 1H), 7.50 (t, J = 7.6 Hz, 1H), 4.79 (s, 2H), 2.34 (s, 3H). ESI-HRMS *m/z* $[M+H]^+$ calculated for $C_{14}H_{10}ClO_3$: 261.0318, found: 261.0313.

*4.1.7. General procedure for the preparation of compounds **2j**–**2s***

To a mixture of aromatic amines (0.46 mmol), KI (10 mg, 0.06 mmol), K_2CO_3 (50 mg, 0.38 mmol) in DMF (5 mL) was added intermediate **8** (100 mg, 0.38 mmol). The resulting mixture was stirred at 55 °C for 1–2 h. After being cooled, the mixture was poured into ice water and the resulting mixture was extracted with EtOAc. The combined organic layer was washed with brine and dried over anhydrous Na_2SO_4, filtered and concentrated to afford a crude product, which was purified through column chromatography over silica gel.

*4.1.7.1. 2-((Phenylamino)methyl)-3-methylnaphtho[1,2-b]furan-4,5-dione (**2j**).* Following the above procedure, treatment of **8** with aniline for 1 h at 55 °C, gave the crude product, which was purified by column chromatography (eluent: Petroleum ether/EtOAc 10:1) to afford **2j** as a dark red solid (60 mg, 50%). m.p. 178–179 °C. ^{1}H NMR (300 MHz, $CDCl_3$) δ: 8.05 (d, J = 6.2 Hz, 1H), 7.63–7.58 (m, 2H), 7.45–7.39 (m, 1H), 7.25–7.19 (m, 2H), 6.78 (t, J = 6.6 Hz, 1H), 6.73–6.70 (m, 2H), 4.35 (s, 2H), 4.02 (brs, 1H), 2.32 (s, 3H). ^{13}C NMR (75 MHz, $CDCl_3$) δ: 180.2, 175.1, 159.2, 151.0, 147.9, 134.8, 129.9, 129.5, 128.9, 128.3, 128.0, 121.7, 121.1, 120.5, 118.8, 113.5, 38.9, 8.4. IR (ν, cm^{-1}): 3232, 2823, 2753, 1665, 1551, 1221, 914, 828, 775. ESI-HRMS *m/z* $[M+Na]^+$ calculated for $C_{20}H_{15}NO_3Na$: 340.0950, found: 340.0944.

*4.1.7.2. 2-(((4-Methoxyphenyl)amino)methyl)-3-methylnaphtho[1,2-b]furan-4,5-dione (**2k**).* Following the above procedure, treatment of **8** with *p*-methoxyphenylamine for 1 h at 55 °C, gave the crude product, which was purified by column chromatography (eluent: Petroleum ether/EtOAc 10:1) to afford **2k** as a dark red solid (29 mg, 22%). m.p. 185–187 °C. ^{1}H NMR (300 MHz, $CDCl_3$) δ: 8.06 (d, J = 9.0 Hz, 1H), 7.67–7.62 (m, 2H), 7.46–7.41 (m, 1H), 6.83 (d, J = 8.1 Hz, 2H), 6.68 (d, J = 6.0 Hz, 2H), 5.12 (s, 1H), 4.32 (s, 2H), 3.87 (s, 1H), 3.77 (s, 3H), 2.32 (s, 3H). ^{13}C NMR (75 MHz, $CDCl_3$) δ: 180.2, 174.8, 160.4, 158.5, 149.1, 143.0, 134.8, 129.9, 129.4, 128.3, 128.0, 121.9, 121.6, 118.7, 114.4, 114.1, 55.0, 39.7, 8.9. IR (ν, cm^{-1}): 3466, 2917, 1672, 1579, 1440, 1246, 848, 771, 594. ESI-HRMS *m/z* $[M+Na]^+$ calculated for $C_{21}H_{17}NO_4Na$: 370.1055, found: 370.1059.

*4.1.7.3. 2-(((4-Methylphenyl)amino)methyl)-3-methylnaphtho[1,2-b]furan-4,5-dione (**2l**).* Following the above procedure, treatment of **8** with *p*-methylphenylamine for 1 h at 55 °C, gave the crude product, which was purified by column chromatography (eluent: Petroleum ether/EtOAc 4:1) to afford **2l** as a dark red solid (38 mg, 30%). m.p. 179–181 °C. ^{1}H NMR (300 MHz, $CDCl_3$) δ: 8.05 (d, J = 7.5 Hz, 1H), 7.69–7.60 (m, 2H), 7.46–7.41 (m, 1H), 7.05 (d, J = 8.4 Hz, 2H), 6.69 (d, J = 8.1 Hz, 2H), 4.34 (s, 2H), 2.31 (s, 3H), 2.27 (s, 3H). ^{13}C NMR (75 MHz, $CDCl_3$) δ: 180.1, 174.9, 159.0, 150.4, 144.3, 134.8, 130.5, 129.9, 129.4, 129.3, 128.3, 128.0, 121.7, 121.2, 120.4, 113.4, 39.3, 19.9, 8.3. IR (ν, cm^{-1}): 3308, 2920, 2356, 1655, 1518, 1221, 908, 773, 690. ESI-HRMS *m/z* $[M+Na]^+$ calculated for $C_{21}H_{17}NO_3Na$: 354.1106, found: 354.1111.

*4.1.7.4. 2-(((4-Chlorophenyl)amino)methyl)-3-methylnaphtho[1,2-b]furan-4,5-dione (**2m**).* Following the above procedure, treatment of **8** with *p*-chlorophenylamine for 2 h at 55 °C, gave the crude product, which was purified by column chromatography (eluent: Petroleum ether/EtOAc 4:1) to afford **2m** as a dark red solid (33 mg, 25%). m.p. 183–184 °C. ^{1}H NMR (300 MHz, $CDCl_3$) δ: 8.05 (d, J = 7.8 Hz, 1H), 7.70–7.62 (m, 2H), 7.49–7.41 (m, 2H), 7.22 (d, J = 7.5 Hz, 2H), 6.81–6.78 (m, 1H), 4.37 (s, 2H), 2.29 (s, 3H). ^{13}C NMR (75 MHz, $CDCl_3$) δ: 180.6, 174.9, 159.1, 150.3, 144.0, 134.8, 130.0, 129.6, 128.8, 128.3, 128.1, 126.2, 121.7, 120.6, 118.9, 114.1, 38.9, 8.4. IR (ν, cm^{-1}): 3304, 1657, 1597, 1489, 1401, 1262, 908, 826, 771. ESI-HRMS *m/z* $[M+H]^+$ calculated for $C_{20}H_{15}ClNO_3$: 352.0735, found: 352.0734.

*4.1.7.5. 2-(((4-Fluorophenyl)amino)methyl)-3-methylnaphtho[1,2-b]furan-4,5-dione (**2n**).* Following the above procedure, treatment of **8** with *p*-fluorophenylamine for 1 h at 55 °C, gave the crude product, which was purified by column chromatography (eluent: Petroleum ether/EtOAc 4:1) to afford **2n** as a dark red solid (42 mg, 33%). m.p. 179–180 °C. ^{1}H NMR (300 MHz, $CDCl_3$) δ: 8.05 (d, J = 7.5 Hz, 1H), 7.68–7.63 (m, 2H), 7.48–7.42 (m, 1H), 6.97–6.90 (m, 2H), 6.69–6.65 (m, 2H), 4.32 (s, 2H), 2.32 (s, 3H). ^{13}C NMR (75 MHz, $CDCl_3$) δ: 180.0, 174.9, 158.9, 156.0 ($^1J_{CF}$ = 235.1 Hz), 150.3, 142.8, 134.8, 129.9, 129.5, 128.3, 127.9, 121.6, 121.2, 117.8, 115.4 ($^2J_{CF}$ = 22.5 Hz), 113.9 ($^3J_{CF}$ = 7.6 Hz), 39.3, 8.5. IR (ν, cm^{-1}): 3332, 2924, 2853, 1663, 1511, 1221, 904, 818, 771. ESI-HRMS *m/z* $[M+Na]^+$ calculated for $C_{20}H_{14}FNO_3Na$: 358.0855, found: 358.0862.

*4.1.7.6. 2-(((3-Methylphenyl)amino)methyl)-3-methylnaphtho[1,2-b]furan-4,5-dione (**2o**).* Following the above procedure, treatment of **8** with *m*-methylphenylamine for 2 h at 55 °C, gave the crude product, which was purified by column chromatography (eluent: Petroleum ether/EtOAc 4:1) to afford **2o** as a dark red solid (38 mg, 30%). m.p. 174–175 °C. ^{1}H NMR (300 MHz, $CDCl_3$) δ: 8.05 (d, J = 7.5 Hz, 1H), 7.68–7.60 (m, 2H), 7.56–7.41 (m, 1H), 7.12 (t, J = 7.5 Hz, 1H), 6.64 (d, J = 7.2 Hz, 1H), 6.57–6.55 (m, 2H), 4.35 (s, 2H), 2.33 (s, 3H), 2.31 (s, 3H). ^{13}C NMR (75 MHz, $CDCl_3$) δ: 180.2, 175.2, 159.1, 150.9, 145.0, 134.8, 134.7, 130.1, 129.9, 129.5, 128.8, 128.6, 121.7, 121.2, 119.5, 117.5, 114.0, 110.3, 38.9, 20.9, 8.4. IR (ν, cm^{-1}): 3320, 2922, 2842, 1670, 1589, 1219, 908, 691. ESI-HRMS *m/z* $[M+Na]^+$ calculated for $C_{21}H_{17}NO_3Na$: 354.1106, found: 354.1111.

*4.1.7.7. 2-(((3-Methoxyphenyl)amino)methyl)-3-methylnaphtho[1,2-b]furan-4,5-quin-one (**2p**).* Following the above procedure, treatment of **8** with *m*-methoxyphenylamine for 2 h at 55 °C, gave the crude product, which was purified by column chromatography (eluent: Petroleum ether/EtOAc 4:1) to afford **2p** as a dark red solid (44 mg, 33%). m.p. 182–183 °C. ^{1}H NMR (300 MHz, $CDCl_3$) δ: 8.04 (d, J = 7.5 Hz, 1H), 7.65–7.62 (m, 2H), 7.44–7.42 (m, 1H), 7.12 (t, J = 7.5 Hz, 1H), 6.34–6.31 (m, 2H), 6.28 (d, J = 2.4 Hz, 1H), 4.34 (s, 2H), 3.78 (s, 3H), 3.76 (s, 1H), 2.33 (s, 3H). ^{13}C NMR (75 MHz, $CDCl_3$) δ: 180.2, 174.9, 161.4, 159.0, 150.7, 149.9, 134.7, 129.8, 129.4, 128.2, 128.0, 121.9, 121.1, 119.1, 117.5, 117.0, 110.2, 109.1, 55.3, 39.1, 8.5. IR (ν, cm^{-1}): 3388, 2922, 1671, 1597, 1158, 904, 782, 687. ESI-HRMS *m/z* $[M+H]^+$ calculated for $C_{21}H_{18}NO_4$: 348.1236, found: 348.1230.

*4.1.7.8. 2-(((3-Chlorophenyl)amino)methyl)-3-methylnaphtho[1,2-b]furan-4,5-dione (**2q**).* Following the above procedure, treatment of **8** with *m*-chlorophenylamine for 1 h at 55 °C, gave the crude product, which was purified by column chromatography (eluent:

Petroleum ether/EtOAc 5:1) to afford **2q** as a dark red solid (48 mg, 36%). m.p. 180–181 °C. ^{1}H NMR (300 MHz, $CDCl_3$) δ 8.06 (d, J = 9.0 Hz, 1H), 7.66–7.62 (m, 2H), 7.46–7.42 (m, 1H), 7.13 (t, J = 8.1 Hz, 1H), 6.77–6.72 (m, 2H), 6.58 (d, J = 2.4 Hz, 1H), 5.12 (s, 1H), 4.35 (s, 2H), 2.34 (s, 3H). ^{13}C NMR (75 MHz, $CDCl_3$) δ: 179.9, 175.2, 159.1, 149.9, 147.7, 134.8, 129.9, 129.8, 129.6, 128.3, 128.1, 121.7, 120.9, 118.9, 117.9, 114.4, 112.4, 110.9, 38.3, 8.4. IR (ν, cm^{-1}): 3323, 2935, 1680, 1569, 1243, 980. ESI-HRMS m/z $[M+H]^+$ calculated for $C_{20}H_{15}ClNO_3$: 352.0740, found: 352.0737.

*4.1.7.9. 2-(((2-Methoxyphenyl)amino)methyl)-3-methylnaphtho[1,2-b]furan-4,5-dione (**2r**).* Following the above procedure, treatment of **8** with *o*-methoxyphenylamine for 1 h at room temperature, gave the crude product, which was purified by column chromatography (eluent: Petroleum ether/EtOAc 20:1) to afford **2r** as a dark red solid (59 mg, 45%). m.p. 180–181 °C. ^{1}H NMR (300 MHz, $CDCl_3$) δ: 8.07 (d, J = 7.5 Hz, 1H), 7.71–7.61 (m, 2H), 7.47–7.42 (m, 1H), 6.94 (t, J = 7.5 Hz, 1H), 6.82–6.78 (m, 3H), 4.40 (s, 2H), 3.88 (s, 3H), 3.84 (s, 1H), 2.33 (s, 3H). ^{13}C NMR (75 MHz, $CDCl_3$) δ: 180.2, 175.1, 159.1, 152.4, 150.0, 134.8, 129.9, 129.5, 128.3, 128.0, 127.3, 123.3, 121.8, 121.2, 120.8, 119.6, 118.2, 109.5, 55.2, 38.9, 8.5. IR (ν, cm^{-1}): 3420, 1641, 1554, 1220, 906, 764, 743, 736. ESI-HRMS m/z $[M+H]^+$ calculated for $C_{21}H_{18}NO_4$: 348.1236, found: 348.1232.

*4.1.7.10. 2-(((2-Chlorophenyl)amino)methyl)-3-methylnaphtho[1,2-b]furan-4,5-dione (**2s**).* Following the above procedure, treatment of **8** with *o*-chlorophenylamine for 1 h at 45 °C, gave the crude product, which was purified by column chromatography (eluent: Petroleum ether/EtOAc 20:1) to afford **2s** as a dark red solid (53 mg, 40%). m.p. 182–183 °C. ^{1}H NMR (300 MHz, $CDCl_3$) δ: 8.07 (d, J = 7.5 Hz, 1H), 7.70–7.60 (m, 2H), 7.48–7.43 (m, 1H), 7.31 (d, J = 1.5 Hz, 1H), 7.24 (t, J = 6.3 Hz, 1H), 6.98–6.92 (m, 1H), 6.85–6.80 (m, 1H), 4.49 (s, 2H), 2.32 (s, 3H). ^{13}C NMR (75 MHz, $CDCl_3$) δ: 180.1, 174.9, 159.1, 149.7, 142.4, 134.8, 129.9, 129.5, 128.9, 128.3, 127.9, 127.4, 122.0, 121.7, 121.2, 120.8, 118.2, 111.2, 38.5, 8.3. IR (ν, cm^{-1}): 3398, 1670, 1600, 1400, 1030, 905, 750. ESI-HRMS m/z $[M+H]^+$ calculated for $C_{20}H_{15}ClNO_3$: 352.0740, found: 352.0736.

4.2. Biology

4.2.1. In vitro NQO1 assay

Ortho-quinones (0.1–50 μmol L^{-1}) were monitored as NQO1 substrates using an NADPH recycling assay and recombinant NQO1 (DT-diaphorase, EC 1.6.5.5, human recombinant, Sigma), in which NADPH oxidation to $NADP^+$ was monitored by absorbance (A_{340} nm) on a Varioskan Flash (Thermo, Waltham, MA). Compounds in DMSO stock (2 μL) were added to a 96 plate. NADPH (400 μmol L^{-1}) and NQO1 (1.4 μg/mL) in 50 mmol·L^{-1}potassium phosphate buffer (pH = 7.4) were added to each well (198 μL). Once the 96-well plate was filled with the assay solutions, except the NADPH solution, it was placed into the instrument and left to sit for 3 min before starting the measurements. The enzyme reaction was initiated by automated dispensing of the NADPH solution into the wells, and data was recorded at 2 s intervals for 5 min at room temperature (22–25 °C). The linear portion of the absorbance *vs* time graphs (the first 20 s to 1 min) were fitted, and the slops were calculated (velocity). NADPH oxidation rates were compared with reactions lacking compound. Initial velocities were calculated and data expressed as μmol NADPH oxidized/min/μmol protein. All reactions were carried out at least in triplicate.

Initial velocities were calculated for a variety of concentrations of **2e**, **2m**, **2n** and β-lap and Michaelis–Menten curves were generated using Graphpad Prism 6.

4.2.2. Molecular modeling

A docking study was performed using the crystal structure of the human NQO1 complex with dicoumarol (PDB code: 2F1O and resolution 2.75 Å) and the structure was editor according to provide a monomer of the protein and protonated use GOLD 5.1. The ligand was then removed to leave the receptor complex, which was used for the subsequent docking studies. For preparation of ligand structures, the selected analogs were energy minimized using MOE 2013.08 with a MMFF94x forcefield using gas phase calculations and a cutoff of 0.01. Charges were then fixed using an MMFF94 forcefield. For computational docking, GOLD 5.1 software was used in combination with ChemScore scoring function. The active site was defined as being any volume within 8 Å of the scaffold of dicoumarol in its crystal pose in 2F1O. The number of genetic algorithm (GA) run was set to 10, and scoring of the docked poses was performed with the ChemScore scoring function. Each GOLD run was saved and the strongest scoring binding pose of each ligand (subject to a rmsd default distance threshold of 1.5 Å) was compared to that of the reference ligand position observed in the crystal structure. The best output poses of the ligands generated were analyzed on the basis of ChemScore, feasibility of hydride transfer process, and H-bonding to the enzyme. The best poses were visualized with MOE 2013.08.

4.2.3. Cell viability assay

Growth inhibition was determined by the MTT colorimetric assay. Cells were plated in 96-well plates at a density of 10,000 cells/mL and allowed to attach overnight (16 h). *Ortho*-quinone solutions were applied in medium for 2 h, removed, and replaced with fresh medium, and the plates were incubated at 37 °C under a humidified atmosphere containing 5% CO_2 for 72 h. MTT (50 μg) was added and the cells were incubated for another 4 h. Medium/MTT solutions were removed carefully by aspiration, the MTT formazan crystals were dissolved in 100 μL of DMSO, and absorbance was determined on a plate reader at 560 nm. When investigating the effect of dicoumarol, cells were cotreated with vehicle or 25 μmol L^{-1} dicoumarol and compound **2n** for 2 h with at least three technical replicates. IC_{50} values (concentration at which cell survival equals 50% of control) were determined from semilog plots of percent of control versus concentration. Selectivity ratios were defined as IC_{50} value for the H596 cell line divided by IC_{50} value for the A549 cell line.

4.2.4. Superoxide generation assays

The reduction of *ortho*-quinones and the resulting was monitored by a spectrophotometric assay in which the rate of reduction of cytochrome *c* was quantified at 550 nm. Briefly, the assay mixture contained cytochrome *c* (30 μmol L−1), reduced nicotinamide adenine dinucleotide (NADPH; 0.2 mmol L^{-1}), recombinant human NQO1 (0.1–3.0 μg/mL) (DT-diaphorase, EC 1.6.5.5, human recombinant, Sigma), and naphthquinones (25 μmol L^{-1}) in a final volume of 1 mL of Tris–HCl (25 mmol L^{-1}, pH 7.4) containing 0.7 mg/mL bovine serum albumin (BSA) and 0.1% Tween-20. Reactions were carried out at room temperature and started by the addition of NADPH. Rates of reduction were calculated from the initial linear part of the reaction curve (0–30 s), and results were expressed in terms of micromoles of cytochrome *c* reduced per minute per milligram of NQO1 by use of a molar extinction coefficient of 21.1 mM^{-1} cm^{-1} for cytochrome *c*. All reactions were carried out at least in triplicate.

Acknowledgments

We are thankful for the financial support of the National Natural Science Foundation of China (No.81302636), the National Natural

Science Foundation of Jiangsu Province of China (No. BK20130656), the Project Program of State Key Laboratory of Natural Medicines, China Pharmaceutical University (No. SKLNMZZ201202), the National Found for Fostering Talents of Basic Science (NFFTBS) of China (No. J1030830) and the fundamental Research Funds for the Central Universities.

Appendix A. Supplementary data

Supplementary data related to this article can be found at http://dx.doi.org/10.1016/j.ejmech.2014.05.041.

References

[1] N. Kongkathip, B. Kongkathip, P. Siripong, C. Sangma, S. Luangkamin, M. Niyomdecha, S. Pattanapa, S. Piyaviriyagul, P. Kongsaeree, Potent anti-tumor activity of synthetic 1,2-naphthoquinones and 1,4-naphthoquinones, Bioorg. Med. Chem. 11 (2003) 3179–3191.
[2] D. Siegel, D.L. Gustafson, D.L. Dehn, J.Y. Han, P. Boonchoong, L.J. Berliner, D. Ross, NAD(P)H: quinone oxidoreductase 1: role as a superoxide scavenger, Mol. Pharmacol. 65 (2004) 1238–1247.
[3] S. Danson, T.H. Ward, J. Butler, M. Ranson, DT-diaphorase: a target for new anticancer drugs, Cancer Treat. Rev. 30 (2004) 437–449.
[4] G.L. David, I. Romieu, J.J. Sienra-Monge, Nicotinamide adenine dinucleotide (phosphate) reduced: quinone oxidoreductase and glutathione S-transferase M1 polymorphisms and childhood asthma, Am. J. Respir. Crit. Care. Med. 168 (2003) 1199–1204.
[5] M. Muller, Polyphenol cytotoxicity induced by the bacterial toxin pyocyanin: role of NQO1, Free Radial Bio. Med. 47 (2009) 84–91.
[6] A. Gellis, H. Kovacic, N. Boufatah, P. Vanelle, Cytosolic, synthesis and cytotoxicity evaluation of some benzimidazole-4,7-diones as bioreductive anticancer agents, Eur. J. Med. Chem. 43 (2008) 1858–1864.
[7] S.M. Planchon, J.J. Pink, C. Tagliarino, W.G. Bornmann, M.E. Varnes, D.A. Boothman, β-Lap-induced apoptosis in human prostate cancer cells: involvement of NQO1/xip3, Exp. Cell. Res. 267 (2001) 95–106.
[8] F.J. Alcaín, J.M. Villalba, NQO1-directed antitumour quinones, Expert Opin. Ther. Patents (2007) 649–665.
[9] D. Siegel, C. Yan, D. Ross, NAD(P)H:quinone oxidoreductase 1 (NQO1) in the sensitivity and resistance to antitumor quinones, Biochem. Pharmacol. 83 (2012) 1033–1040.
[10] M.A. Colucci, C.J. Moody, G.D. Couch, Natural and synthetic quinones and their reduction by the quinone reductase enzyme NQO1: from synthetic organic chemistry to compounds with anticancer potential, Org. Biomol. Chem. 6 (2008) 637–656.
[11] D. Kostrzewa-Nowak, M.J. Paine, A. Korytowska, K. Serwatka, S. Piotrowska, C.R. Wolf, J. Tarasiuk, Bioreductive activation of mitoxantrone by NADPH cytochrome P450 reductase. Implications for increasing its ability to inhibit the growth of sensitive and multidrug resistant leukaemia HL60 cell, Cancer Lett. 245 (2007) 252–262.
[12] E.I. Parkinson, J.S. Bair, M. Cismesia, P.J. Hergenrother, Efficient NQO1 substrates are potent and selective anticancer agents, ACS Chem. Biol. 8 (2013) 2173–2183.
[13] M. Hassani, W. Cai, K.H. Koelsch, D.C. Holley, A.S. Rose, F. Olang, J.P. Lineswala, W.G. Holloway, J.M. Gerdes, M. Behforouz, H.D. Beall, Lavendamycin antitumor agents: structure-based design, synthesis, and NAD(P)H: quinone oxidoreductase 1 (NQO1) model validation with molecular docking and biological studies, J. Med. Chem. 51 (2008) 3104–3115.
[14] M. Hassani, W. Cai, D.C. Holley, J.P. Lineswala, B.R. Maharjan, G.R. Ebrahimian, H. Seradj, M.G. Stocksdale, F. Mohammadi, C.C. Marvin, J.M. Gerdes, H.D. Beall, M. Behforouz, Novel Lavendamycin analogues as antitumor agents: synthesis, in vitro cytotoxicity, structure-metabolism, and computational molecular modeling studies with NAD(P)H: quinone oxidoreductase 1, J. Med. Chem. 48 (2005) 7733–7749.
[15] W. Cai, W. Hassani, R. Karki, E.D. Walter, K.H. Koelsch, H. Seradj, J.P. Lineswala, H. Mirzaei, J.S. York, F. Olang, M. Sedighi, J.S. Lucas, T.J. Eads, A.S. Rose, S. Charkhzarrin, N.G. Hermann, H.D. Beall, M. Behforouz, Synthesis, metabolism and in vitro cytotoxicity studies on novel lavendamycin antitumor agents, Bioorg. Med. Chem. 18 (2010) 1899–1909.
[16] E.A. Bey, M.S. Bentle, K.E. Reinicke, Y. Dong, C.R. Yang, Girard, an NQO1-and PARP-1-mediated cell death pathway induced in non-small-cell lung cancer cells by β-lap, Proc. Natl. Acad. Sci. USA 104 (2007) 11832–11837.
[17] F. Liu, G. Yu, G. Wang, H. Liu, X. Wu, Q. Wang, M. Liu, K. Liao, M. Wu, X. Cheng, H. Hao, An NQO1-initiated and p53-independent apoptotic pathway determines the anti-tumor effect of tanshinone IIA against non-small cell lung cancer, PloS One 7 (2012) e42138.
[18] J. Bian, B. Deng, X. Zhang, T. Hu, N. Wang, W. Wang, H. Pei, Y. Xu, H. Chu, X. Li, H. Sun, Q. You, Lewis acid mediated highly regioselective intramolecular cyclization for the synthesis of β-lapachone, Tetrahedron Lett. 55 (2014) 1475–1478.
[19] M.S. Bentle, K.E. Reinicke, E.A. Bey, D.R. Spitz, Boothman, calcium-dependent modulation of poly (ADP-ribose) polymerase-1 alters cellular metabolism and DNA repair, J. Biol. Chem. 281 (2006) 33684–33696.
[20] X. Cheng, F. Liu, T. Yan, X. Zhou, L. Wu, K. Liao, G. Wang, H. Hao, Metabolic profile, enzyme kinetics, and reaction phenotyping of β-Lapachone metabolism in human liver and intestine in vitro, Mol. Pharmacol. 12 (2012) 3476–3485.
[21] G. Asher, O. Dym, P. Tsvetkov, J. Adler, Y. Shaul, The crystal structure of NAD(P)H quinone oxidoreductase 1 in complex with its potent inhibitor dicoumarol,, Biochemistry 45 (2006) 6372–6378.
[22] M.L. Verdonk, J.C. Cole, M.J. Hartshorn, C.W. Murray, R.D. Taylor, Improved protein-ligand docking using GOLD, Proteins: Struct. Funct. Genet. 52 (2003) 609–623.
[23] K.A. Nolan, J.R. Doncaster, M.S. Dunstan, K.A. Scott, A.D. Frenkel, D. Siegel, R.A. Bryce, Synthesis and biological evaluation of coumarin-based inhibitors of NAD(P)H: quinone oxidoreductase-1 (NQO1), J. Med. Chem. 52 (2009) 7142–7156.
[24] M. Faig, M.A. Bianchet, P. Talalay, S. Chen, S. Winski, D. Ross, L.M. Amzel, Structures of recombinant human and mouse NAD(P)H: quinone oxidoreductases: species comparison and structural changes with substrate binding and release, Proc. Natl. Acad. Sci. USA 97 (2000) 3177–3182.
[25] M. Faig, M.A. Bianchet, S. Winski, R. Hargreaves, C.J. Moody, A.R. Hudnott, L.M. Amzel, Structure-based development of anticancer drugs: complexes of NAD(P)H: quinone oxidoreductase 1 with chemotherapeutic quinones, Structure 9 (2001) 659–667.
[26] M.A. Bianchet, M. Faig, L.M. Amzel, Structure and mechanism of NAD[P]H: quinone acceptor oxidoreductases (NQO), Meth. Enzymol. 382 (2004) 144–174.
[27] K. Ramanathan, V. Shanthi, R. Sethumadhavan, Exploring the role of C-H….π interactions on the structural stability of membrane proteins, Int. J. Pharm. Bio. Sci. 1 (2010) 1–14.
[28] M.F. Mendoza, N.M. Hollabaugh, S.U. Hettiarachchi, R.L. McCarley, Human NAD(P)H: quinone oxidoreductase type I (hNQO1) activation of quinone propionic acid trigger groups, Biochemistry 51 (2012) 8014–8026.
[29] Version 2013.08, Molecular Operating Environment, Chemical Computing Group, Montreal, QC, 2013.
[30] J.J. Newsome, M.A. Colucci, M. Hassani, H.D. Beall, C. Moody, Benzimidazole- and benzothiazole-quinones: excellent substrates for NAD(P)H:quinone oxidoreductase 1, J. Org. Biomol. Chem. 5 (2007) 3665–3673.
[31] M.M. Tarpey, D.A. Wink, M.B. Grisham, Methods for detection of reactive metabolites of oxygen and nitrogen: in vitro and in vivo considerations, Am. J. Physiol. Regul. Integr. Comp. Physiol. 286 (2004) R431–R444.
[32] C. Pidathala, R. Amewu, B. Pacorel, G.L. Nixon, P. Gibbons, W.D. Hong, S.C. Leung, N.G. Berry, R. Sharma, P.A. Stocks, A. Srivastava, A.E. Shone, S. Charoensutthivarakul, L. Taylor, O. Berger, A. Mbekeani, A. Hill, N.E. Fisher, A.J. Warman, G.A. Biagini, S.A. Ward, P.M. O'Neill, Identification, design and biological evaluation of bisaryl quinolones targeting *Plasmodium falciparum* type II NADH: quinone oxidoreductase (PfNDH2), J. Med. Chem. 55 (2012) 1831–1843.